Acta Neuropathologica (2022) 144:521–536
https://doi.org/10.1007/s00401-022-02462-z

ORIGINAL PAPER

Decreased FAK activity and focal adhesion dynamics impair proper neurite formation of medium spiny neurons in Huntington's disease

Hae Nim Lee[1,2] · Seung Jae Hyeon[1] · Heejung Kim[1,2] · Kyoung Mi Sim[1] · Yunha Kim[1] · Jeongmin Ju[1,3] · Junghee Lee[4] · Yingxiao Wang[5] · Hoon Ryu[1] · Jihye Seong[1,2,3]

Received: 25 March 2022 / Revised: 11 June 2022 / Accepted: 25 June 2022 / Published online: 20 July 2022

Abstract

Huntington's disease (HD) is a neurodegenerative disorder caused by a polyglutamine expansion in the protein huntingtin (HTT) [55]. While the final pathological consequence of HD is the neuronal cell death in the striatum region of the brain, it is still unclear how mutant HTT (mHTT) causes synaptic dysfunctions at the early stage and during the progression of HD. Here, we discovered that the basal activity of focal adhesion kinase (FAK) is severely reduced in a striatal HD cell line, a mouse model of HD, and the human post-mortem brains of HD patients. In addition, we observed with a FRET-based FAK biosensor [59] that neurotransmitter-induced FAK activation is decreased in HD striatal neurons. Total internal reflection fluorescence (TIRF) imaging revealed that the reduced FAK activity causes the impairment of focal adhesion (FA) dynamics, which further leads to the defect in filopodial dynamics causing the abnormally increased number of immature neurites in HD striatal neurons. Therefore, our results suggest that the decreased FAK and FA dynamics in HD impair the proper formation of neurites, which is crucial for normal synaptic functions [52]. We further investigated the molecular mechanism of FAK inhibition in HD and surprisingly discovered that mHTT strongly associates with phosphatidylinositol 4,5-biphosphate, altering its normal distribution at the plasma membrane, which is crucial for FAK activation [14, 60]. Therefore, our results provide a novel molecular mechanism of FAK inhibition in HD along with its pathological mechanism for synaptic dysfunctions during the progression of HD.

Keywords Huntington's disease · Focal adhesion kinase (FAK) · Huntingtin · Focal adhesion dynamics · Neurites · PtdIns(4,5)P_2

Introduction

Huntington's disease (HD) is a neurodegenerative disorder characterized by motor, cognitive, and psychiatric dysfunctions [55]. HD is caused by an expansion of CAG repeats in the huntingtin gene, which results in abnormally long (usually over 36) polyglutamine (poly Q) in the N-terminal of the protein huntingtin (HTT) [34]. Mutant huntingtin (mHTT) proteins are misfolded and tend to aggregate, accumulating in nuclear inclusions and dystrophic neurites [10]. While the effect of insoluble mHTT inclusions on cell viability is controversial [1, 31, 57], emerging evidence suggests that mHTT aggregates are associated with the gain of toxic functions in HD [10, 38, 44]. For example, mHTT aggregates can block the normal transcription process in the nucleus [26, 41] and disrupt neuritic transport in neurites, leading to dystrophic neurites and synaptic dysfunctions [15, 39]. In addition, mHTT can cause a loss of normal functions of

Hae Nim Lee and Seung Jae Hyeon contributed equally to this work.

✉ Hoon Ryu
hoonryu@kist.re.kr

✉ Jihye Seong
jseong@kist.re.kr

1 Brain Science Institute, Korea Institute of Science and Technology (KIST), Seoul 02792, Republic of Korea

2 Department of Converging Science and Technology, Kyung Hee University, Seoul 02453, Republic of Korea

3 Division of Bio-Medical Science & Technology, KIST School, Korea University of Science and Technology, Seoul 02792, Republic of Korea

4 Department of Neurology, Boston University Alzheimer's Disease Center, Boston University School of Medicine, Boston, MA 02118, USA

5 Department of Bioengineering, University of California, San Diego, CA 92093, USA

huntingtin, which is suggested to be involved in a variety of cellular processes, such as the transport of organelles, gene transcription, autophagy, cell adhesion and motility [33, 58, 68]. In particular, molecular complexes related to cell adhesion are reported to be altered in neurons expressing mHTT [68], implying that mHTT may prevent the normal development and maintenance of neuronal processes [67, 68]. Neurite dynamics are crucial for the formation of synapses and thus neuronal functions in the brain [43]; however, the molecular and cellular mechanisms by which mHTT impacts cell adhesion and motility and neurite dysfunction are still unclear.

Cell adhesion and motility are regulated by cytoskeletal and focal adhesion (FA) dynamics [47, 66]. Focal adhesion is a specialized microdomain at the plasma membrane where a cell directly senses the extracellular environment through a transmembrane receptor integrin and many structural and signaling molecules [7, 48]. Focal adhesions are also important to physically connect to the cytoskeleton and transfer the extracellular signals to inside the cells [7]. Focal adhesion kinase (FAK) is a crucial signaling molecule at FAs and is composed of a FERM (protein 4.1, ezrin, radixin, and moesin homology) domain, a kinase domain, and a focal adhesion targeting (FAT) domain [47]. Upon the binding of extracellular matrix (ECM), integrins are activated and clustered, which causes autophosphorylation at FAK Tyr397 at FAs. For the full activation of FAK, the basic patch of the FAK FERM domain is required to bind to PtdIns(4,5)P_2 at the plasma membrane [14, 60], and Src kinase, which is recruited to phosphorylated Tyr397 via its SH2 domain, further phosphorylates FAK at Tyr576 and Tyr577. The activated FAK-Src complex then recruits and activates other FA components, such as p130Cas and paxillin [48]. Thus, FAK is a key molecule for the regulation of FA dynamics.

FAK functions in neurite motility in response to extracellular cues during neuronal development [8, 52]. Thus, in FAK-deficient mice or neurons, growth cone shape and dynamics, neuritogenesis, axonal arborization, and neuronal migration are impaired [9, 16, 72]. While the functions of FAK in neuronal development have been previously studied [9, 52], its pathophysiological role in Huntington's disease is not yet clear. Here, we report markedly decreased FAK activity in a stable HD cell line, a transgenic mouse HD model, and human post-mortem brains of HD patients. We discovered that the decreased FAK activity in HD striatal neurons impairs FA dynamics and this results in improper neurite formation, which is essential for synaptic functions in the brain [52]. We further investigated the molecular mechanism of FAK inhibition in HD. Downregulated FAK activity in HD can be directly induced by the acute introduction of mHTT. We discovered that mHTT aggregates can strongly associate with phosphatidylinositol 4,5-biphosphate (PtdIns(4,5)P_2), altering its normal distribution, which is crucial for FAK activation. These results suggest a novel molecular and pathophysiological mechanism of dystrophic neurites in Huntington's disease.

Materials and methods

Plasmids and transfection

The FRET-based FAK biosensor was previously described [59]. In brief, it is composed of a membrane-targeting motif (M**G**CIKSKRKDNLNDDE), ECFP, SH2 domain, a flexible linker (GSTSGSGKPGSGEGS), a FAK substrate peptide (ETDD**Y**AEIIDE), and YPet. mCherry-tagged paxillin, FAK-related non-kinase (FRNK), and a constitutively active mutant (CA FAK) were previously described [59, 60]. mTagBFP2-tagged paxillin was constructed by inserting a PCR product of mTagBFP2 in the C-terminus of paxillin in the pRK5 vector. PrimeSTAR HS DNA polymerase (Takara) and In-Fusion (Clontech) were used for subcloning. Plasmids containing normal and mutant HTT (HTT Q2 vs. HTT Q62 and HTT Q25-GFP vs. HTT Q103-GFP) were previously constructed and validated [21, 35, 64]. We constructed HTT Q25- or HTT Q103-mTagBFP2 by replacing GFP in the HTT Q25-GFP or HTT Q103-GFP construct with a PCR product of mTagBFP2. The GFP-PLC PH domain was previously described [63]. For transient expression of the plasmids in the cultured cells, the plasmids were transfected into the cells using Lipofectamine™ 2000 reagent (Invitrogen) according to the manufacturer's protocol.

Cell culture and reagents

The ST*Hdh*$^{Q7/7}$ (Q7) and ST*Hdh*$^{Q111/111}$ (Q111) cell lines [37, 69] were maintained in DMEM supplemented with 10% fetal bovine serum (HyClone), 1 unit per ml penicillin, and 100 µg per ml streptomycin. Cell culture reagents were purchased from HyClone. Cells were cultured in a 95% humidity, 5% CO_2 incubator at 33 °C. Carbachol (CCL) was purchased from Sigma, and phalloidin was purchased from Invitrogen.

Preparation of human tissues and immunohistochemistry

Control and HD human brain samples were obtained from the Boston University Alzheimer's Disease Center (BUADC) and Genome Science Institute (BUGSI). Information of normal subjects and HD striatal tissue samples is provided in Supplementary Table 1 [Online Resource 1]. The neuropathological stage of HD was determined based on Dr. Vonsattel's grading system [73]. Next of kin provided informed consent for participation and brain donation. The

study was performed in accordance with institutional regulatory guidelines.

Post-mortem brain tissues were sectioned in a coronal plane at 20 µm. We used human striatal tissues according to the following coordinates: caudate ($X = -12 \pm 2$, $Y = 14 \pm 2$, $Z = 14 \pm 2$), putamen ($X = -24 \pm 2$, $Y = 14 \pm 2$, $Z = 2 \pm 2$), thickness: 20 µm. The tissue sections were heat-mediated antigen retrieval performed by submerging the slides in Tris–EDTA buffer (pH 9.0). Then, the sections were blocked with blocking solution (5% BSA) and incubated with p-FAK (Y397) (1:200 dilutions; Abcam, #ab81298) for 24 h. After three washes, the slides were processed with a Vector ABC Kit (Vector Lab). The immunoreactive signals were developed with DAB chromogen (Thermo Fisher Scientific) and analyzed under bright field microscopy.

Animals and virus injection

Mice were purchased from the Jackson Laboratory (Bar Harbor, ME, USA) and maintained as a colony at the KIST SPF Animal Facility. YAC128 mice were bred with females from their background strain (B6CBAFI/J), and offspring were genotyped using PCR. All mice were weighed at 3 weeks of age and equally distributed according to weight and percentage within each cohort. These procedures were performed in accordance with Guide for the Care and Use of Laboratory Animals guidelines. Information on the wild-type and HD mouse models is provided in Supplementary Table 2 [Online Resource 1].

Brain specimens of mice were prepared as previously described [20, 30, 35]. AAV-Q25-GFP and AAV-Q103-GFP virus was injected by a stereotaxic microinjector (Stoelting Co.) at 12 months of age. AAVs were delivered into the striatum (AP: 0.86 mm, ML: ± 2 mm, DV: 2.9 mm) of wild-type mice (C57BL/6 J) as previously described [21]. Control groups were injected with AAV-Q25-GFP. Neuropathological analysis was performed 2 weeks after injection. All animal experiments and in vitro studies of animal tissues were performed in accordance with the National Institutes of Health Guide for the Care and Use of Laboratory Animals. The animal study was approved by KIST IACUC (Institutional Animal Care and Use Committee) (Approval Number: 2018–009).

Immunofluorescence

Immunofluorescence staining for p-FAK (Y397) in the HD animal model was performed as previously described [36]. Animal experiments were performed in accordance with the *Guide for the Care and Use of Laboratory Animals* guidelines and approved by KIST animal care committees. The tissue sections were preincubated with blocking solution (5% BSA) and incubated with anti-p-FAK (Y397) antibody (1:200 dilutions; Abcam, ab81298) for 24 h. After three washes, the slides were incubated with fluorescence-conjugated secondary antibodies. The nuclei were counterstained with DAPI (4',6-diamidino-2-phenylindole). Images were captured using a Nikon A1 confocal microscope**.**

For the immunostaining of cultured cells, Q7 and Q111 cells were fixed with 4% paraformaldehyde for 10 min and permeabilized with 0.1% Triton X-100 for 5 min. Cells were incubated in 1% BSA in PBS for 1 h, and then with mouse anti-FAK (phospho-Y397) antibody (5 µg/ml, Abcam, #ab81298) or mouse anti-PtdIns(4,5)P_2 antibody (10 µg/ml, Echelon, #Z-P045) overnight at 4 °C. After three washes with PBS, the cells were incubated with goat anti-mouse antibody conjugated to Alexa Fluor 488 (diluted 1:200) for 1.5 h. After three washes with PBS for 10 min each, the stained cells were observed under a Nikon Ti-E fluorescence microscopy.

Western blotting

For western blotting, a total of 30 µg of protein was subjected to SDS–PAGE and blotted with anti-phospho Y397 FAK antibody (1:1000 dilution, Cell Signaling, #8556). Equal amounts of protein were loaded and detected, and expression levels were normalized to that of β-actin (1:1000 dilution, Santa Cruz Biotechnology, #sc-47778) on the same membrane. We developed western blot membranes with enhanced chemiluminescence (ECL) solution, and images were captured with a luminescent image analyzer LAS-4000 mini (FUJIFILM). The quantification of band intensity on the blot was analyzed with a software program, Multi Gauge V3.0 (FUJIFILM).

FRET image acquisition

For fluorescence imaging, the cells were prepared on coverglass-bottom dishes (SPL) coated with 10 µg/ml fibronectin (Invitrogen). Images were collected by a Nikon Ti-E inverted microscope and a cooled charge-coupled device camera using NIS software (Nikon). For FRET imaging of the FAK biosensor, we used a 438DF24 excitation filter, a 458DRLP dichroic mirror, and two emission filters controlled by a filter changer (438DF24 for ECFP and 542DF27 for FRET). The fluorescence intensity of non-transfected cells was quantified as the background signal and subtracted from the fluorescent signal on transfected cells. The pixel-by-pixel ratio images of ECFP/FRET were calculated based on the

background-subtracted fluorescence intensity images of ECFP and FRET by the NIS program to allow the quantification and statistical analysis of FRET responses.

TIRF imaging and focal adhesion analysis

For the imaging of focal adhesions, Q7 and Q111 cells were transfected with mCherry-paxillin to allow the identification of FAs. At 24 h post-transfection, cells were serum-starved in DMEM supplemented with 0.5% FBS, 1 unit per ml penicillin, and 100 µg per ml streptomycin overnight. The cells were then stimulated with 20 µM carbachol and imaged with either the epifluorescence microscope described above or a total reflection fluorescence (TIRF) microscope (Nikon) equipped with a fiber-coupled 561 nm laser. FA quantification was performed using the Focal Adhesion Analysis Server [4]. FAs were detected and outlined by thresholding the highlight images, and their numbers were analyzed from binary images using the spot detection function in the NIS program.

Super-resolved structured illumination microscopy (SR-SIM)

For super-resolved structured illumination microscopy (SR-SIM) imaging, Q7 cells expressing HTT Q103-GFP were fixed with 4% paraformaldehyde for 10 min and permeabilized with 0.1% Triton X-100 for 5 min. Cells were incubated in 1% BSA in PBS for 1 h and then with mouse anti-PtdIns(4,5)P_2 antibody (10 µg/ml, Echelon, #Z-P045) overnight at 4 °C. After three washes with PBS, the cells were incubated with goat anti-mouse antibody conjugated to Alexa Fluor 488 (diluted 1: 200) for 1.5 h. After three washes with PBS for 10 min each, the stained cells were observed under an Elyra 7 microscope (Zeiss) with a 60 × objective. The 3D SIM images were obtained every 1 µm along the z-axis and then aligned (3D) and reconstructed with the Zeiss Zen 3.0 SR (black) program. Dual iterative SIM (SIM^2), a nonlinear iterative reconstruction algorithm developed by Zeiss, was used to reconstruct the images.

Statistical analysis

All data are shown as the mean ± standard error of the mean (s.e.m.). The significance of differences between groups was calculated using a two-tailed Student's t-test or one-way ANOVA followed by post hoc Sidak's multiple comparisons test (GraphPad Prism 8). For categorical variables, data were analyzed using Fisher's exact test (Social Science Statistics). A significant difference was determined by $p < 0.05$.

Results

FAK activity is reduced in an HD cell line, a transgenic mouse HD model, and post-mortem human brains of patients with HD

We first performed immunohistochemistry to check the level of active FAK (FAK pY397) in human post-mortem brains of control subjects and HD patients. The p-FAK immunoreactivity found in the cytosolic compartment of striatal neurons of a control subject was surprisingly reduced in HD patients (Fig. 1a). The densitometry analysis of p-FAK immunoreactivity confirmed that p-FAK levels were significantly reduced in the caudate and putamen of HD patients (Fig. 1b, c). Next, we compared the p-FAK level in the brain sections of control mice and the HD transgenic mouse YAC128. The results showed that p-FAK immunoreactivity was markedly decreased in the striatal neurons of the YAC128 mouse brain (Fig. 1d, e), suggesting that FAK activity is reduced in the HD mouse model.

We then investigated whether FAK activity is decreased in the HD stable striatal cell line STHdhQ111/Q111 (Q111) compared to its control, STHdhQ7/Q7 (Q7). Again, the level of phospho-tyrosine 397 was significantly lower in the HD cell line (Fig. 1f, g). The levels of p-FAK in Q7 and Q111, as measured by western blotting, also confirmed the significantly reduced p-FAK level in Q111 (Fig. 1h, i). Additionally, we confirmed the reduction in p-FAK levels in HD patient fibroblast-derived induced neurons (Supplementary Fig. 1 [Online Resource 1]). These results indicate that basal FAK activity is severely impaired in the stable cell line, transgenic mouse model, and human post-mortem brains of HD.

The expression of mHTT in the mouse striatum and striatal cell line leads to decreased FAK activity

To verify whether the transduction of mHTT also alters FAK activity, we delivered AAV-HTT Q25-EGFP or AAV-HTT Q103-EGFP into the striatal region of the mouse brain (Fig. 2a). In agreement with previous results (Fig. 1), the level of p-FAK intensity in the neurons expressing AAV-Q103-EGFP decreased approximately twofold compared to that in the neurons expressing AAV-Q25-EGFP (Fig. 2b, c). These results indicate that mHTT can downregulate the level of FAK activity in HD.

We further investigated whether the acute introduction of mHTT can directly affect FAK activity. When comparing the p-FAK levels in Q7 cells transiently expressing

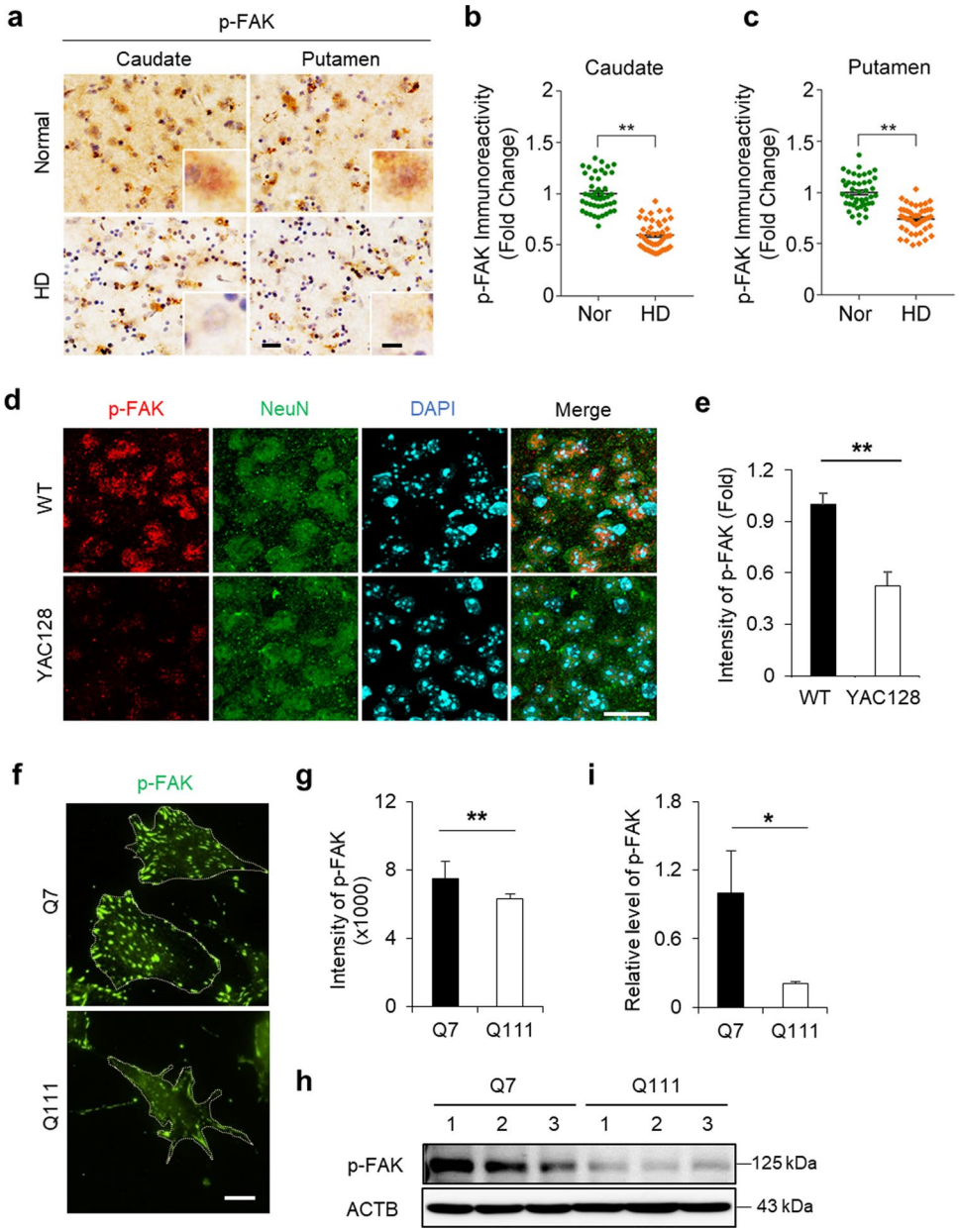

Fig. 1 The reduced FAK activity in post-mortem brains, transgenic mouse model, and striatal cell line of HD. **a** Immunohistochemistry images of p-FAK levels in caudate and putamen of normal and HD patient post-mortem brain. Scale bar: 20 µm (left) and 5 µm (right). **b-c** The densitometry analysis of p-FAK immunoreactivity of striatal neurons in the post-mortem brains of normal (Nor) and HD patients. Data are shown as mean ± s.e.m. Statistical significance: *t*-test, $^{**}p < 0.005$, $n = 50$ cells per group. **d** Immunofluorescence staining of p-FAK in wild-type and YAC128 HD mouse model. NeuN staining identifies neurons, and the nuclei were stained with DAPI. Scale bar: 20 µm. **e** Bar graph shows the averaged fluorescence intensity of p-FAK in YAC128 HD mouse model. Data are shown as mean ± s.e.m. Statistical significance: *t*-test, $^{**}p < 0.005$, $n = 30$ cells per group. **f** Immunofluorescence staining of p-FAK in Q7 and Q111 cells. Scale bar: 20 µm. **g** Bar graph shows the averaged fluorescence intensity of p-FAK in Q7 and Q111 cells. Data are shown as mean ± s.e.m. Statistical significance: t-test, $^{*}p < 0.005$, $n = 20$ cells per group. **h** The expression levels of p-FAK in Q7 and Q111 cells. **i** The p-FAK level was quantified by densitometry analysis and normalized to β-actin. Data are shown as mean ± s.e.m. Statistical significance: t-test, $^{*}p < 0.05$, $n = 3$

normal huntingtin (HTT Q2) or mutant huntingtin (HTT Q62) (Fig. 2d), we found that the intensity of p-FAK was significantly reduced in cells expressing HTT Q62 (Fig. 2e, f). The reduced p-FAK level was also confirmed by western blotting (Fig. 2g, h). Taken together, our results suggest that mHTT downregulates the level of FAK activity.

The FRET-based FAK biosensor identifies impaired FAK activation upon treatment with neurotransmitters in HD striatal cells

To measure the levels of FAK activity in live cells, we used the FAK biosensor based on fluorescence resonance energy transfer (FRET) [59]. The FAK FRET biosensor is composed of a specific substrate for FAK and an SH2 domain between the FRET pair ECFP and YPet (Fig. 3a). When active FAK phosphorylates the substrate tyrosine in the biosensor, the phosphorylated substrate subsequently binds to the intramolecular SH2 domain, causing a conformational change of the biosensor. This then causes a decrease in FRET between ECFP and YPet; thus, the ECFP/FRET emission ratios of the FAK biosensor can indicate FAK activity in live cells.

Utilizing this FRET-based FAK biosensor, we first confirmed that basal FAK activity is significantly reduced in the HD cell line Q111 compared to Q7 cells (Fig. 3b, c). We also observed that the ECFP/FRET ratios of the FAK biosensor

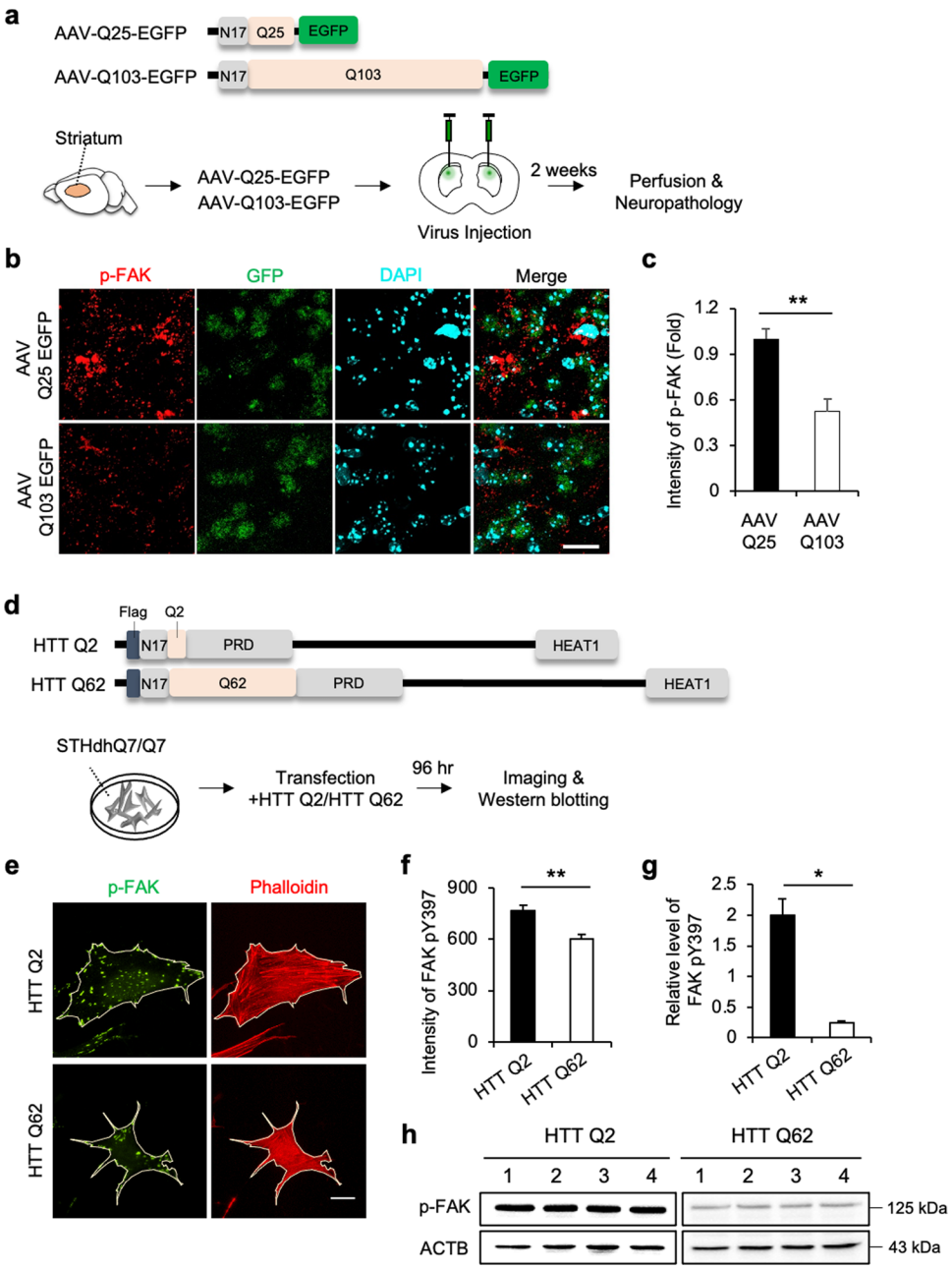

Fig. 2 Mutant huntingtin (mHTT) decreases the basal FAK level both in the mouse striatum and the striatal cell lines. **a** A scheme of AAV-Q25-EGFP and AAV-Q103-EGFP constructs and in vivo delivery viruses into the striatum of WT mice. **b** Immunofluorescence staining of p-FAK in AAV- Q25 and AAV-Q103. Scale bar: 20 µm. **c** Bar graph shows the averaged fluorescence intensity of p-FAK in AAV-Q25 and AAV-Q103. Data are shown as mean ± s.e.m. Statistical significance: t-test, $^{**}p < 0.005$, $n = 30$ cells per group. **d** A scheme of HTT Q2 and HTT Q62 constructs and transient expression of HTT into the Q7 cells. **e, f** Immunofluorescence staining of p-FAK and phalloidin in HTT Q2- or HTT Q62-expressing Q7 cells **e**. Scale bar: 20 µm. Bar graph in **f** shows the averaged fluorescence intensity of p-FAK phalloidin in HTT Q2- or HTT Q62-expressing Q7 cells ($n = 61$ and 62). Data are shown as mean ± s.e.m. Statistical significance: *t*-test, $^{**}p < 0.005$. **g, h** The expression levels of p-FAK in HTT Q2- and HTT Q62-expressing Q7 cells (**g**). The p-FAK level was quantified by densitometry analysis and normalized to β-actin (**f**). Data are shown as mean ± s.e.m. Statistical significance: t-test, $^{*}p < 0.05$, $n = 4$

in Q7 cells decreased with the addition of a FAK-negative mutant (FAK-related non-kinase, FRNK), and a constitutively active mutant (CA FAK) recovered the reduced FAK level in Q111 cells (Fig. 3a–c). We confirmed the correlation between these ECFP/FRET ratios and the levels of phosphorylated FAK Y397 (Fig. 3d).

We next compared FAK activation in Q7 and Q111 cells upon treatment with the cholinomimetic drug carbachol. Acetylcholine is a crucial neurotransmitter for the function of striatal neurons [3]. It has been shown that the carbachol-induced activation of the muscarinic acetylcholine (M1) receptor can induce FAK phosphorylation, and FAK activation is blocked by siRNA for the M1 receptor [6, 29], suggesting a link between the M1 receptor and FAK activation. When we measured the FRET changes of the FAK biosensor in response to carbachol, the ECFP/FRET level of the FAK biosensor in Q7 cells was increased upon treatment with carbachol, while a much-reduced FRET change was observed in Q111 cells (Fig. 3e–g and Supplementary Video. 1 [Online Resource 2]). Therefore, in addition to the reduced basal FAK level in Q111 (Fig. 3b, c), the carbachol-induced FAK activation is impaired in the striatal cells of HD.

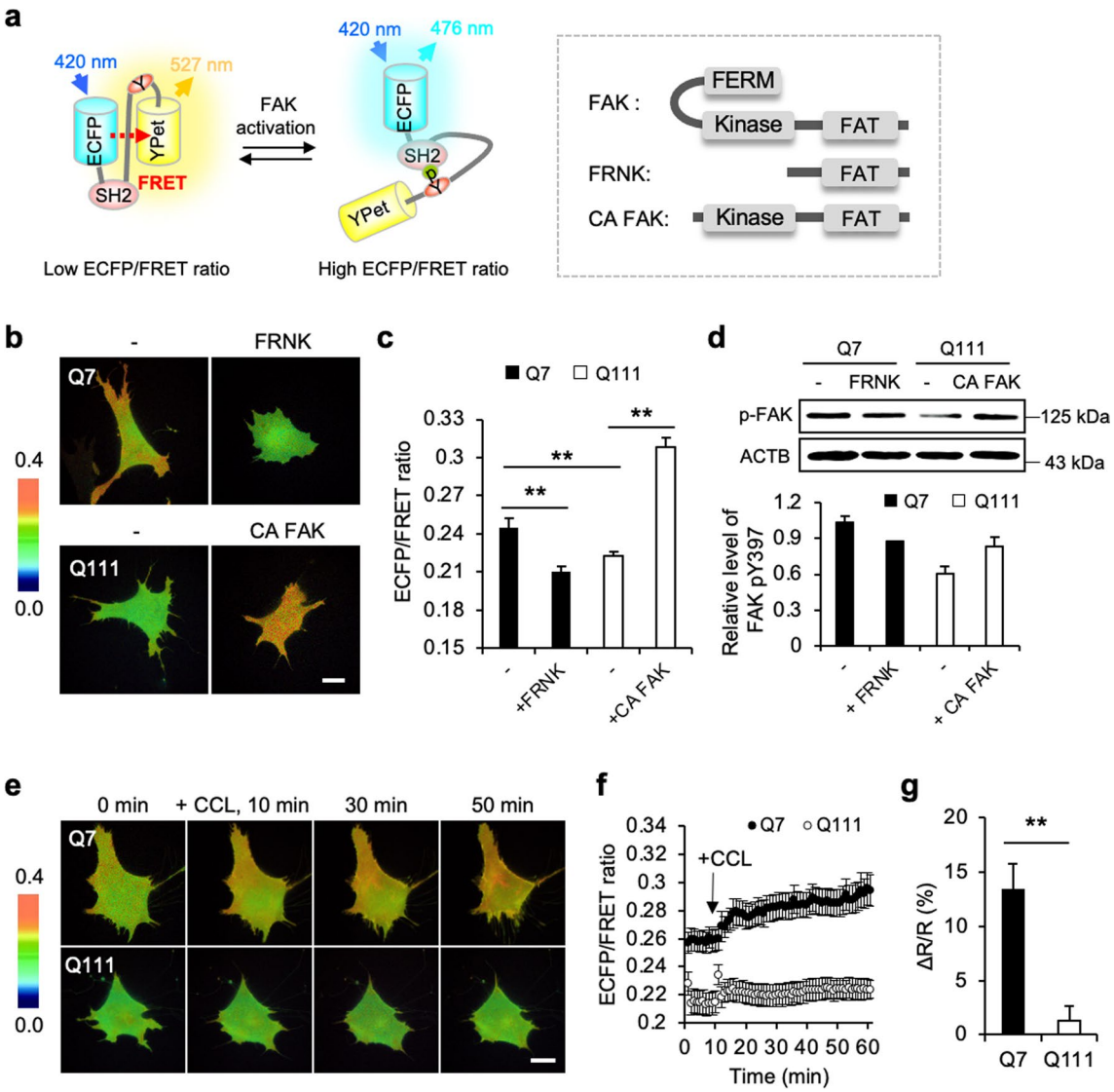

Fig. 3 Neurotransmitter-induced FAK activation and focal adhesion disassembly are defective in HD striatal cells. **a** Scheme of the FRET-based FAK biosensor. FAK induced-phosphorylation of tyrosine residue (indicated as Y) on the biosensor triggers a conformational change in the biosensor which leads to the FRET ratio change. Schematic depictions of wild type FAK, its negative mutant (FRNK), and a constitutive active mutant (CA FAK) are shown in the box. **b, c** The representative ECFP/FRET ratio images **b** and the quantified ECFP/FRET ratios of the FAK biosensor **c** in Q7 or Q111 cells expressing without or with FRNK or CA FAK cells Scale bar: 20 µm. Data are shown as mean ± s.e.m. ($n = 18$, 42, 17 and 18 cells). Statistical significance: one-way ANOVA with sidak's multiple comparisons test, $^{*}p < 0.05$, $^{**}p < 0.005$. **d** The expression levels of p-FAK in Q7 and Q111 cells transfected without or with FRNK or CA FAK. The p-FAK level was quantified by densitometry analysis and normalized to β-actin. Data are shown as mean ± s.e.m. $n = 3$. **e–g** The representative images **e** and time-course graph of the ECFP/FRET ratio **f** of the FAK biosensor in Q7 and Q111 cells after the treatment of 20 µM carbachol (CCL) for indicated times. Scale bar: 20 µm. The bar graph in **g** shows the maximal ECFP/FRET ratio changes of the FAK biosensor in Q7 and Q111 after the treatment of 20 µM carbachol. Data are represented as mean ± s.e.m. ($n = 10$ and 12 cells). Statistical significance: *t*-test, $^{**}p < 0.005$

Reduced FAK activity impairs focal adhesion dynamics in HD striatal cells

FAK serves as a key regulator of focal adhesion (FA) dynamics, which is critical in cell adhesion, migration, and neuronal development [47, 52, 66]. Thus, we next investigated whether the reduced FAK activity influences the FA dynamics in HD striatal cells. Utilizing the FAK biosensor and mCherry-tagged paxillin, a representative scaffolding protein at focal adhesions [70], we observed the time-dependent changes in FA dynamics after carbachol-mediated FAK activation in Q7 cells but not in Q111 cells (Supplementary Fig. 2 [Online Resource 1]). In response to carbachol, paxillin-positive FAs were disassembled

in Q7 cells, resulting in a change in local FAK activity at these sites (Supplementary Fig. 2a and 2c [Online Resource 1]). In contrast, no detectable change in either paxillin or the FAK biosensor was observed in Q111 cells, suggesting that the reduced FAK activity in HD striatal cells may lead to impaired focal adhesion dynamics (Supplementary Fig. 2b-c [Online Resource 1]).

For the more accurate quantification of focal adhesion dynamics, we monitored mCherry-paxillin in Q7 and Q111 cells by total internal reflection fluorescence (TIRF) microscopy and analyzed them from the Focal Adhesion Analysis Server (FAAS) [4] (Supplementary Fig. 3 [Online Resource 1]). Our results show that Q111 cells display more FAs than Q7 control cells (Fig. 4a, b), and carbachol-induced FA disassembly is significantly inhibited in Q111 cells (Fig. 4a, c and Supplementary Video. 2 [Online Resource 3]). These results confirm that FA dynamics is impaired in HD striatal cells.

To demonstrate that the impaired FA dynamics in HD striatal cells is due to the reduced FAK activity, we first introduced the negative FAK mutant FRNK to Q7 cells and observed that the number of FAs was increased in the Q7 cells expressing FRNK (Fig. 4a and d). In addition, the carbachol-induced disassembly of focal adhesions was

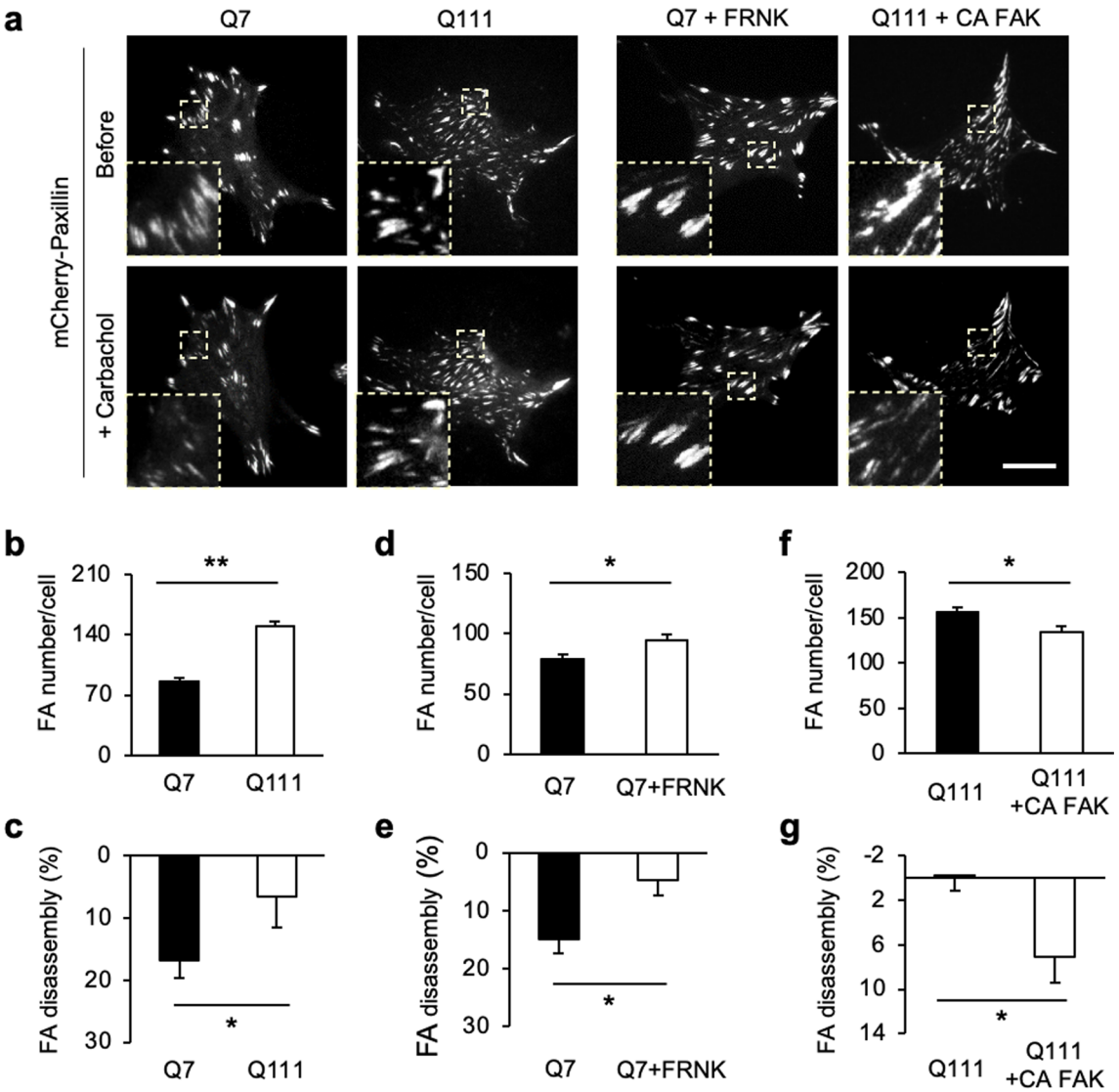

Fig. 4 Decreased FAK activity is associated with the impairment of focal adhesion dynamics in HD striatal cells. **a** The representative TIRF images of mCherry-paxillin in Q7, Q111, Q7 cells expressing FRNK, and Q111 cells expressing CA FAK, before and after 20 μM carbachol stimulation. Scale bar: 20 μm. Insets show the boxed areas at high magnification. **b–g** Bar graphs show the quantification of FA number per cell **b, d** and **f** and FA disassembly rate in response to 20 μM carbachol (**c, e** and **g**) in the indicated groups ($n = 38$, 40 in Fig. 4b, c; $n = 39$, 38 in Fig. 4d, e; $n = 75$, 66 in Fig. 4f, g). Data are shown as mean ± s.e.m. Statistical significance: *t*-test, $^{*}p < 0.05$, $^{**}p < 0.005$

also severely inhibited by FRNK (Fig. 4a and e), suggesting that FAK activity is crucial for FA dynamics. Next, we introduced a constitutively active mutant CA FAK in Q111 cells to determine whether it could rescue the impaired FA dynamics in Q111 cells. Indeed, the number of FAs decreased with the reconstitution of FAK (Fig. 4a, f), and carbachol-induced FA disassembly was also recovered in Q111 cells expressing CA FAK (Fig. 4a, g). These results suggest that the reduced FAK activity impairs the FA dynamics in HD striatal cells.

Impaired FA dynamics blocks proper development of neuronal projections in HD striatal cells

In normal cells, FAK and paxillin are mainly located at focal adhesions in the filopodial shaft and regulate the dynamics of filopodia [23, 53]. In contrast, filopodial tips contain more dynamic focal complexes that contain only a small percentage of mature adhesion components. It has been suggested that the dynamic focal complex contains p-FAK, but not paxillin, and as paxillin follows, this focal complex becomes stable and larger focal adhesions stabilizing filopodia [19, 23, 45]. Interestingly, we observed reduced focal adhesion dynamics at filopodial projections in striatal cells expressing mutant HTT. When we compared the levels of p-FAK and paxillin, p-FAK was often observed without paxillin at the tips of the projections in HTT Q2-expressing cells (Fig. 5a, c, d and Supplementary Fig. 4a [Online Resource 1]), indicating that they are small and dynamic focal complexes. In contrast, in HTT Q62-expressing cells, larger and mature focal adhesions containing both p-FAK and paxillin were detected at the tips of the projections (Fig. 5b–d and Supplementary Fig. 4b [Online Resource 1]). These data suggest impaired FA dynamics at the projections in HD, possibly as a result of the delay or arrest of filopodial retraction.

The reduced FA dynamics at neuronal projections in HD may contribute to the impaired development of neurites in striatal neurons. Indeed, we observed an increased number of shorter neurites in rat primary striatal neurons expressing HTT Q103 compared to HTT Q25 (Fig. 5e–g), suggesting impaired development of neurites in HD. We further monitored the neuronal projections during the adhesion process of the Q7 and Q111 cell lines. We detected a significantly larger number of cellular projections in Q111 cells than in Q7 cells after 2 h of adhesion, and this difference was sustained until 96 h (Fig. 5h, i). The lengths of projections in Q7 and Q111 cells were similar at 2 h of adhesion. However, after 96 h, the neuronal projections in Q7 cells became significantly longer, while those in Q111 cells remained short (Fig. 5h, j). These results suggest that the selection and proper development of neuronal projections are impaired in HD striatal cells.

To confirm that the impaired development of neuronal projections in HD cells is related to the reduced FAK activity, we introduced FRNK or CA FAK and then checked whether the numbers and lengths of neuronal projections can be controlled by FAK activity. The results showed that in HTT Q2-expressing cells, FRNK overexpression led to an increased number of short neurites (Fig. 5k, l). These results suggest that the reduced FAK activity and impaired FA dynamics block the proper development of neuronal projections in HD striatal neurons.

The reduced FAK activity in HD is related to the altered distribution of PtdIns(4,5)P_2 by mHTT

We learned that the reduced FAK activity in HD striatal cells is related to the impairment of FA dynamics and proper development of neurites. We further wondered how FAK activity is initially altered by mHTT in HD striatal cells. First, we checked whether mHTT physically interacts with FAK. The results showed that GFP-tagged normal huntingtin, HTT Q25-GFP, was distributed over the cell with no particular colocalization with FAK. In contrast, HTT Q103-GFP was concentrated in a few bright spots, indicating the aggregation of mHTT, but mHTT also did not directly interact with FAK (Supplementary Fig. 5a [Online Resource 1]). We confirmed that the level of p-FAK was reduced by mHTT (Supplementary Fig. 5b–d [Online Resource 1]).

For the activation of FAK, it is known that a basic region in the FERM domain of FAK binds to phosphatidylinositol 4,5-bisphosphate, PtdIns(4,5)P_2, which induces a partially open conformation of FAK and its autophosphorylation at Y397 [14, 60]. Indeed, mutations in the basic region in the FAK FERM domain disable the activation of FAK [14, 60]. Interestingly, HTT can bind to acidic phospholipids via its N-terminal basic sequences, and in particular, it has been shown that PtdIns(4,5)P_2 can associate more strongly with mHTT [25, 27, 28]. Thus, we next investigated the association between HTT and PtdIns(4,5)P_2 in control and mHTT-expressing cells.

Again, we observed that HTT Q25 is distributed over the cell, while HTT Q103 is aggregated inside the cells (Fig. 6a, b). In HTT Q25-expressing cells, PtdIns(4,5)P_2 was mostly located at the edge of the plasma membrane (Fig. 6a, c). Surprisingly, we observed that mHTT aggregates were surrounded by PtdIns(4,5)P_2 in HTT Q103-expressing cells (Fig. 6b, c), suggesting a strong association between PtdIns(4,5)P_2 and mHTT. We also observed PtdIns(4,5)P_2-positive clusters adjacent to mHTT aggregates in HTT Q103-expressing medium spiny neurons of the striatal region of the mouse brain, which was confirmed (Supplementary Fig. 6 [Online Resource 1]). To confirm the association between PtdIns(4,5)P_2 and mHTT aggregates in striatal Q7 cells expressing HTT Q103-mTagBFP, we further utilized super resolved structured illumination microscopy (SR-SIM). As shown in Fig. 6d, e and Supplementary Video. 3 [Online Resource 4], three-dimensional (3D) SR-SIM images

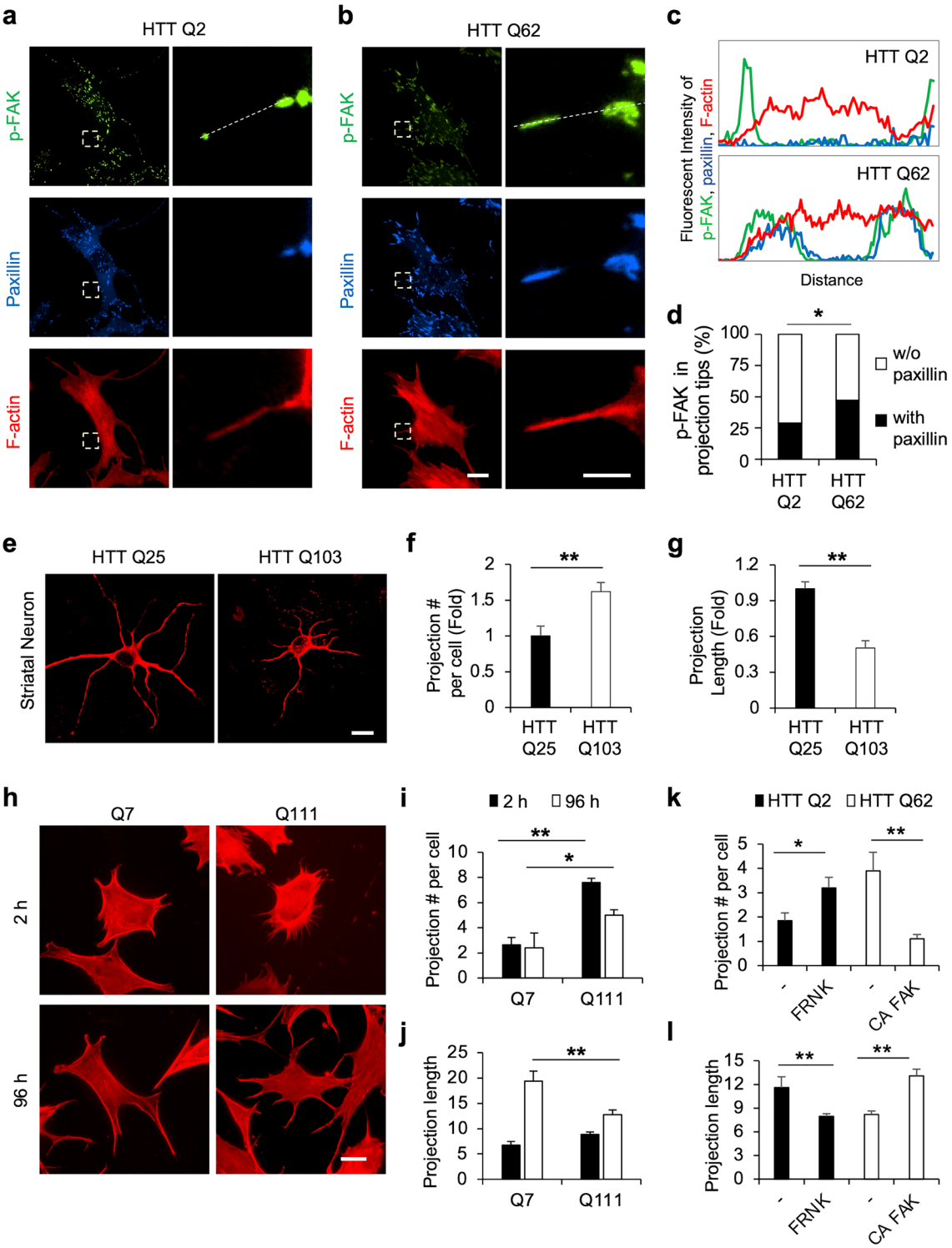

showed that mHTT aggregates are tightly surrounded by a shell of PtdIns(4,5)P_2. These data indicate that mHTT aggregates are strongly associated with PtdIns(4,5)P_2, thus possibly interfering with its normal distribution and function.

We next investigated whether the abnormal distribution of PtdIns(4,5)P_2 in HD cells is linked to impaired FA dynamics. First, we found PtdIns(4,5)P_2 puncta around p-FAK in HTT Q25-expressing cells (Fig. 6f and Supplementary Fig. 7a [Online Resource 1]), suggesting that they can function as mediators of FAK activation. In contrast, we observed that HTT Q103 induced the accumulation of PtdIns(4,5)P_2 surrounding mHTT aggregates in the cytosol but not focal adhesions and significantly decreased

◂**Fig. 5** mHTT impairs the focal adhesion dynamics and proper development of cellular projections. **a–c** Immunofluorescence staining of p-FAK (green), paxillin (blue), and phalloidin (red) in the striatal cell line expressing HTT Q2 **a** or HTT Q62 **b**. Right images show the boxed areas in the left images at high magnification. Scale bar: 5 µm (left) and 20 µm (right). The distribution of p-FAK, paxillin, and F-actin in filopodia (from tip to base) was assessed with line intensity profiles in **c**. **d** The proportion of p-FAK distribution with or without paxillin at the tip of the projections in HTT Q2- or HTT Q62-expressing cells ($n=62$ and 60 cells). Statistical significance: Fisher's exact test, *p < 0.05. **e–g** Immunofluorescence staining of MAP2 in the AAV-HTT Q25 or AAV-HTT Q103 transduced rat striatal neurons **e**. Scale bar: 20 µm. Bar graph in **f** shows the averaged projection number in AAV-HTT Q25 or AAV-HTT Q103-transduced rat striatal neurons. Data are shown as mean ± s.e.m. $n=20$ cells per group. Statistical significance: t-test, $^{**}p<0.005$. Bar graph in **g** shows the averaged projection length in AAV-HTT Q25 and AAV-HTT Q103-transduced rat striatal neurons. Data are shown as mean ± s.e.m. $n=20$ cells per group. Statistical significance: t-test, $^{**}p<0.005$. **h-j** Immunofluorescence staining of phalloidin in Q7 and Q111 cells after adhesion for 2 h or 96 h **h**. Scale bar: 20 µm. Corresponding graphs show the averaged projection number per cell **i** and the averaged projection length **j** in Q7 and Q111 cells ($n=8$, 13, 15, 18 in Fig. 5i; $n=21$, 29, 114, 90 in Fig. 5j). Data are shown as mean ± s.e.m. Statistical significance: one-way ANOVA with sidak's multiple comparisons test, $^{*}p<0.05$, $^{**}p<0.005$. **k-l** Bar graphs show the averaged projection number per cell **k** and the averaged projection length **l** in the striatal cell line expressing HTT Q2, HTT + FRNK, HTT Q62, or HTT Q62 + CA FAK ($n=20$, 35, 20, 45 in Fig. 5k; $n=37$, 112, 77, 49 in Fig. 5l). Data are represented as mean ± s.e.m. Statistical significance: one-way ANOVA with sidak's multiple comparisons test, $^{*}p<0.05$, $^{**}p<0.005$

p-FAK levels (Fig. 6g and Supplementary Fig. 7b [Online Resource 1]). These results suggest that the altered distribution of PtdIns(4,5)P_2 may result in reduced FAK activity.

Next, we introduced mCherry-paxillin and GFP-tagged PLC PH domain, a specific biosensor for the visualization of the real-time dynamics of PtdIns(4,5)P_2 in live cells [63]. In response to carbachol, we observed the local distribution of PtdIns(4,5)P_2 near disassembling FAs in Q7, but no such dynamics was detected in Q111 cells (Fig. 6h, i, Supplementary Fig. 8 [Online Resource 1] and Supplementary Video. 4 [Online Resource 5]). Our results suggest that mHTT aggregates can alter the normal distribution and function of PtdIns(4,5)P_2, which is crucial for the activation of FAK and FA dynamics (Fig. 7). Therefore, mHTT-induced dysregulation of PtdIns(4,5)P_2 can cause reduced FAK activity, which is linked to the impairment of FA dynamics and the abnormal development of neuronal projections in HD striatal cells.

Discussion

Focal adhesion dynamics is required for neurite outgrowth and remodeling during neuronal development and adult neurogenesis [13]. The formation of presynaptic structures in developing axons is initiated by the emergence of axonal filopodia at the tips of growth cones [61, 74]. In the postsynaptic part, dendritic filopodia search for presynaptic axonal partners and evolve into spines to form a stable synaptic connection [11, 24]. These neuronal filopodia are dynamic protrusions with short lifetimes. They are actin-rich thin processes that search the environment [17]; in particular, at the tip of protrusions, neuronal filopodia contact the extracellular matrix through highly dynamic focal complexes [17, 22]. Many of these focal complexes disappear, resulting in the retraction of neuronal filopodia, while some are selected to become more stable focal adhesions supporting the extension of functional neurites [13]. This selection process mediated by FA dynamics is thus important for the proper development of neurites and correct synaptic functions [56].

In HD, the dysregulation of synaptic function and plasticity have been reported [46, 50, 51, 71], which are associated with abnormal density or morphology, and stabilization of dendritic or axonal branches and spines [12, 32, 40]. In this study, we discovered that FAK activity is significantly reduced in a striatal HD cell line, a mouse HD model, and human post-mortem brains of HD patients (Fig. 1). In addition, carbachol-induced FAK activation is impaired in HD striatal cells (Fig. 3), which results in the dysfunction of focal adhesion dynamics (Fig. 4). The decreased FA dynamics causes a defect in filopodial dynamics, which can lead to an increased number of short neurites (Fig. 5). These results are supported by previous studies showing that FAK can control axonal branching and synapse formation and that the depletion of FAK induces the reversion of mature dendritic spines to immature filopodia-like neuronal protrusions [49, 54, 62]. Thus, our results suggest that reduced FAK activity and impaired FA dynamics block proper neurite development and synaptic functions in HD.

An intriguing question is why FAK activity is initially reduced in HD. In particular, the decreased FAK activity can be directly induced by mHTT (Fig. 2); thus, we further investigated the fundamental pathological mechanisms of HD. In the inactive state of FAK, the FERM domain interacts with the kinase domain, and this autoinhibitory interaction is a key mechanism for negatively modulating FAK activity [42]. Upon cell adhesion and integrin clustering, FAK can be recruited to focal adhesion sites via its FAT domain, initiating autophosphorylation at Y397. For full FAK activation, the basic patch of the FERM domain is further required to bind to PtdIns(4,5)P_2 at the plasma membrane [14, 60], which can partially open the closed structure of autoinhibited FAK and maintain the active conformation of FAK [14]. Interestingly, we discovered that mHTT can strongly associate with PtdIns(4,5)P_2, causing the alteration of its normal distribution, which thus blocks FAK activation. In mHTT-expressing cells, PtdIns(4,5)P_2 is abnormally found and sequestered in the cytosol surrounding mHTT aggregates, and the dynamics of PtdIns(4,5)P_2 is severely

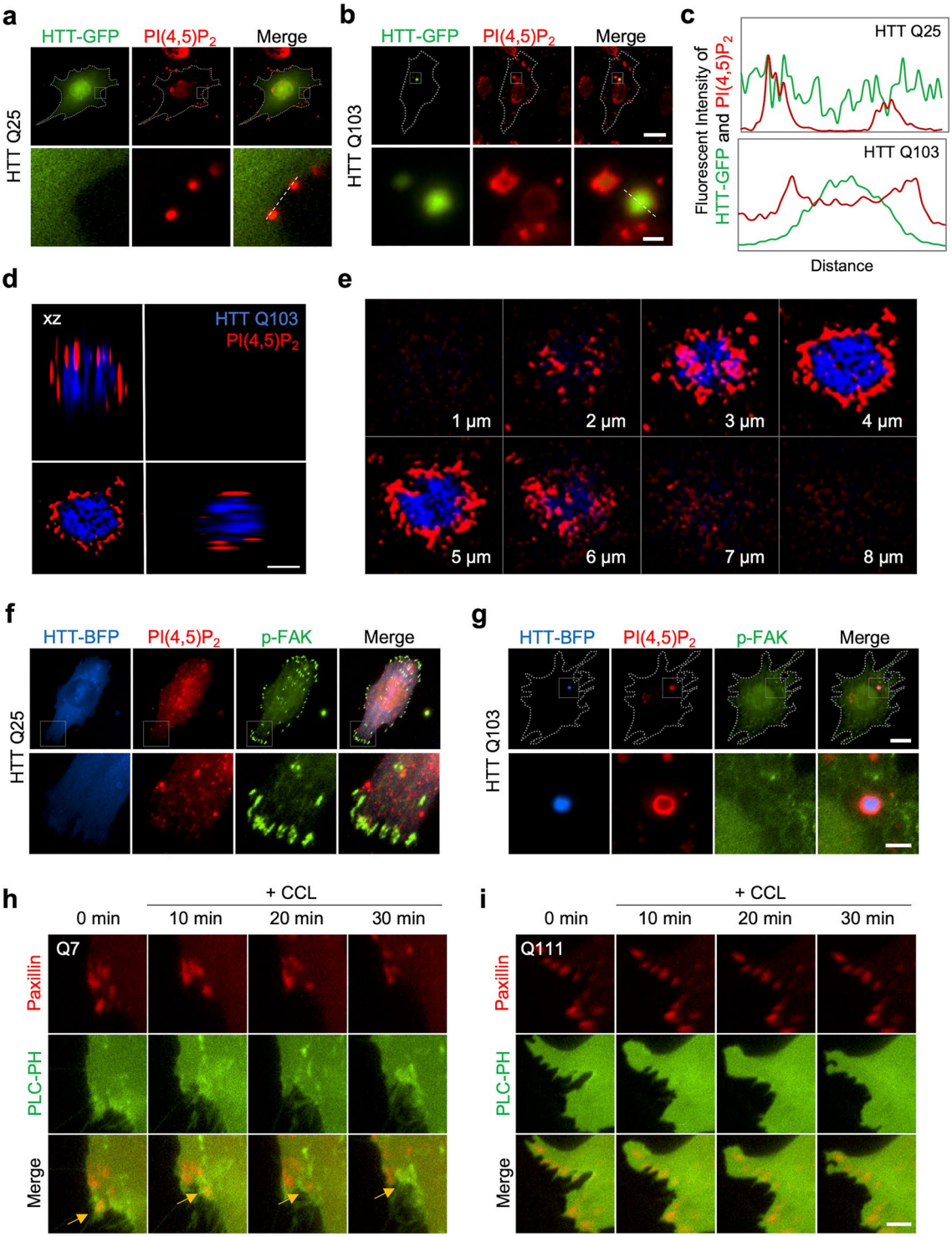
a
HTT-GFP
PI(4,5)P2
Merge
HTT Q25
b
HTT-GFP
PI(4,5)P2
Merge
HTT Q103
c
HTT Q25
HTT Q103
Fluorescent Intensity of HTT-GFP and PI(4,5)P2
Distance
d
xz
HTT Q103
PI(4,5)P2
e
1 μm
2 μm
3 μm
4 μm
5 μm
6 μm
7 μm
8 μm
f
HTT-BFP
PI(4,5)P2
p-FAK
Merge
HTT Q25
g
HTT-BFP
PI(4,5)P2
p-FAK
Merge
HTT Q103
h
+ CCL
0 min
10 min
20 min
30 min
Q7
Paxillin
PLC-PH
Merge
i
+ CCL
0 min
10 min
20 min
30 min
Q111
Paxillin
PLC-PH
Merge

◂**Fig. 6** mHTT binds to PtdIns(4,5)P_2, altering the normal distribution and function of PtdIns(4,5)P_2 for FA dynamics. **a–c** Immunofluorescence staining of HTT (green), PtdIns(4,5)P_2 (red), and merged images in the striatal cell line expressing HTT Q25-GFP **a** or HTT Q103-GFP **b**. Lower images show the boxed areas in the upper images at high magnification. Scale bar: 20 µm (upper) and 2 µm (lower). The distribution of p HTT Q25 or Q103 and PtdIns(4,5)P_2 was assessed with line intensity profiles in **c**. **d, e** Super-resolved SIM images of immunofluorescence staining of HTT Q103-mTagBFP (blue) and PtdIns(4,5)P_2 (red) in the striatal Q7 cells expressing HTT Q103-mTagBFP. The merged xz and yz stacked **f** or z-stack images **g** of an mHTT aggregate. The z-stack depth is labeled in the lower right in each image. Scale bar: 2 µm. **f, g** Immunofluorescence staining of HTT (blue), PtdIns(4,5)P_2 (red), p-FAK (green) and merged images in the striatal cell line expressing HTT Q25-GFP **f** or HTT Q103-GFP **g**. Lower images show the boxed areas in the upper images at high magnification. Scale bar: 20 µm (upper) and 5 µm (lower). **h, i** Time-course images of mCherry-paxillin (red) and GFP-PLC PH domain (green) after the treatment of 20 µM carbachol for indicated times. Yellow arrows in **h** indicate that the GFP-PLC PH domain is recruited to the sites of focal adhesion disassembly. Scale bar: 5 µm

impaired in regulating focal adhesion disassembly (Fig. 6). It is currently unclear how PtdIns(4,5)P_2 is associated with mHTT aggregates and further biophysical and biochemical investigations are needed to clarify the mechanism of this association. One attractive possibility is that the N-terminal basic residues of HTT, which have been suggested to be relevant in the association of acidic phospholipids [5, 28, 65], may mediate such interaction. These results indicate that the mHTT-induced loss of PtdIns(4,5)P_2 function may lead to dysregulation of FAK and FA dynamics in HD.

In conclusion, we report that reduced FAK activity and impaired FA dynamics can result in the failure of proper neurite development in HD, which is critical for synaptic functions in the brain. We also discovered that mHTT directly and strongly associates with PtdIns(4,5)P_2, which is critical for FAK activation, thus resulting in reduced FAK activity and FA dynamics (Fig. 7). The roles of FAK in focal adhesion dynamics have been previously highlighted in growth cone guidance during neural development [9, 54]. In this study, we provide direct evidence of how FAK function is linked to the pathological mechanisms underlying the impaired development of neurites and altered synaptic functions in HD. The alteration in FAK function may further contribute to a variety of neurodevelopmental abnormalities in HD, as recent studies

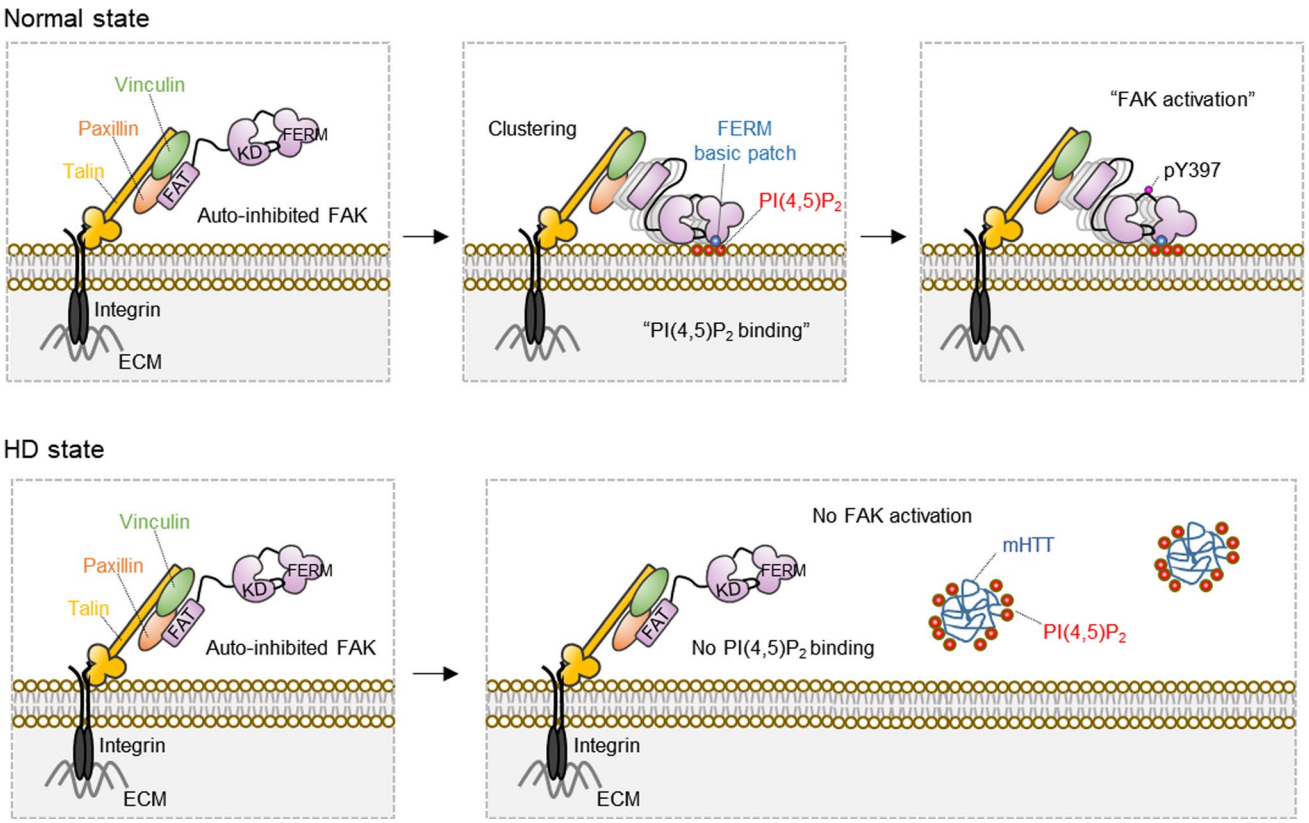

Fig. 7 Proposed model of the impaired FAK activity in HD. (Normal state) Upon cell adhesion and integrin clustering, the autoinhibited FAK is recruited and clustered at focal adhesion sites. The basic patch in the FERM domain of FAK binds to PtdIns(4,5)P_2 at the plasma membrane, leading to the FAK activation. (HD state) Upon cell adhesion and integrin clustering, the autoinhibited FAK can be recruited to focal adhesion sites. mHTT is directly and strongly associated with PtdIns(4,5)P_2 blocking its normal distribution and function for the FAK activation. This leads to the reduced FAK activity in HD

have reported defects in neuronal migration [2] as well as developmental malformations [18] in HD. Therefore, our novel findings will help us to understand the pathophysiological mechanism and investigate strategies to overcome these defects in HD.

Supplementary Information The online version contains supplementary material available at https://doi.org/10.1007/s00401-022-02462-z.

Acknowledgements This work was supported in part by National Research Foundation of Korea grant 2021R1A2C1093429, KIST Institutional grant 2E31523, and Samsung Research Funding & Incubation Center of Samsung Electronics under Project Number SRFC-TC2003-02 (J.S.). This work was also supported by NIH grant R01NS109537 (J.L.), National Research Foundation of Korea grant NRF-2020M3E5D9079742, and KIST Institutional grant 2E31505 (H.R.).

Author contributions JS and HR designed research; HNL, SJH, HK, KMS, YK, JJ performed experiments; JS, HR, HNL, SJH, JL, YW analyzed data; JS, HR, HNL wrote the manuscript.

Declarations

Conflict of interests The authors declare no conflict of interest.

References

1. Arrasate M, Mitra S, Schweitzer ES, Segal MR, Finkbeiner S (2004) Inclusion body formation reduces levels of mutant huntingtin and the risk of neuronal death. Nature 431:805–810. https://doi.org/10.1038/nature02998
2. Barnat M, Capizzi M, Aparicio E, Boluda S, Wennagel D, Kacher R et al (2020) Huntington's disease alters human neurodevelopment. Science 369:787–793. https://doi.org/10.1126/science.aax3338
3. Benarroch EE (2012) Effects of acetylcholine in the striatum. Recent Insights Therapeutic Implications Neurol 79:274–281. https://doi.org/10.1212/WNL.0b013e31825fe154
4. Berginski ME, Gomez SM (2013) The Focal Adhesion Analysis Server: a web tool for analyzing focal adhesion dynamics. F1000Res 2: 68 https://doi.org/10.12688/f1000research.2-68.v1
5. Burke KA, Kauffman KJ, Umbaugh CS, Frey SL, Legleiter J (2013) The interaction of polyglutamine peptides with lipid membranes is regulated by flanking sequences associated with huntingtin. J Biol Chem 288:14993–15005. https://doi.org/10.1074/jbc.M112.446237
6. Calandrella SO, Barrett KE, Keely SJ (2005) Transactivation of the epidermal growth factor receptor mediates muscarinic stimulation of focal adhesion kinase in intestinal epithelial cells. J Cell Physiol 203:103–110. https://doi.org/10.1002/jcp.20190
7. Carragher NO, Frame MC (2004) Focal adhesion and actin dynamics: a place where kinases and proteases meet to promote invasion. Trends Cell Biol 14:241–249. https://doi.org/10.1016/j.tcb.2004.03.011
8. Chacon MR, Fazzari P (2011) FAK: dynamic integration of guidance signals at the growth cone. Cell Adh Migr 5:52–55
9. Chacon MR, Navarro AI, Cuesto G, del Pino I, Scott R, Morales M et al (2012) Focal adhesion kinase regulates actin nucleation and neuronal filopodia formation during axonal growth. Development 139:3200–3210. https://doi.org/10.1242/dev.080564
10. DiFiglia M, Sapp E, Chase KO, Davies SW, Bates GP, Vonsattel JP et al (1997) Aggregation of huntingtin in neuronal intranuclear inclusions and dystrophic neurites in brain. Science 277:1990–1993. https://doi.org/10.1126/science.277.5334.1990
11. Fiala JC, Feinberg M, Popov V, Harris KM (1998) Synaptogenesis via dendritic filopodia in developing hippocampal area CA1. J Neurosci 18:8900–8911
12. Fiala JC, Spacek J, Harris KM (2002) Dendritic spine pathology: cause or consequence of neurological disorders? Brain Res Brain Res Rev 39:29–54. https://doi.org/10.1016/s0165-0173(02)00158-3
13. Fischer RS, Lam PY, Huttenlocher A, Waterman CM (2019) Filopodia and focal adhesions: an integrated system driving branching morphogenesis in neuronal pathfinding and angiogenesis. Dev Biol 451:86–95. https://doi.org/10.1016/j.ydbio.2018.08.015
14. Goni GM, Epifano C, Boskovic J, Camacho-Artacho M, Zhou J, Bronowska A et al (2014) Phosphatidylinositol 4,5-bisphosphate triggers activation of focal adhesion kinase by inducing clustering and conformational changes. Proc Natl Acad Sci USA 111:E3177-3186. https://doi.org/10.1073/pnas.1317022111
15. Gunawardena S, Her LS, Brusch RG, Laymon RA, Niesman IR, Gordesky-Gold B et al (2003) Disruption of axonal transport by loss of huntingtin or expression of pathogenic polyQ proteins in Drosophila. Neuron 40:25–40. https://doi.org/10.1016/s0896-6273(03)00594-4
16. Gupton SL, Gertler FB (2010) Integrin signaling switches the cytoskeletal and exocytic machinery that drives neuritogenesis. Dev Cell 18:725–736. https://doi.org/10.1016/j.devcel.2010.02.017
17. Heckman CA, Plummer HK 3rd (2013) Filopodia as sensors. Cell Signal 25:2298–2311. https://doi.org/10.1016/j.cellsig.2013.07.006
18. Hickman RA, Faust PL, Rosenblum MK, Marder K, Mehler MF et al (2021) Developmental malformations in Huntington disease: neuropathologic evidence of focal neuronal migration defects in a subset of adult brains. Acta Neuropathol 141:399–413. https://doi.org/10.1007/s00401-021-02269-4
19. Hu YL, Lu S, Szeto KW, Sun J, Wang Y, Lasheras JC et al (2014) FAK and paxillin dynamics at focal adhesions in the protrusions of migrating cells. Sci Rep 4:6024. https://doi.org/10.1038/srep06024
20. Hwang YJ, Han D, Kim KY, Min SJ, Kowall NW, Yang L et al (2014) ESET methylates UBF at K232/254 and regulates nucleolar heterochromatin plasticity and rDNA transcription. Nucleic Acids Res 42:1628–1643. https://doi.org/10.1093/nar/gkt1041
21. Hyeon SJ, Park J, Yoo J, Kim SH, Hwang YJ, Kim SC et al (2021) Dysfunction of X-linked inhibitor of apoptosis protein (XIAP) triggers neuropathological processes via altered p53 activity in Huntington's disease. Prog Neurobiol 204:102110. https://doi.org/10.1016/j.pneurobio.2021.102110
22. Jacquemet G, Hamidi H, Ivaska J (2015) Filopodia in cell adhesion, 3D migration and cancer cell invasion. Curr Opin Cell Biol 36:23–31. https://doi.org/10.1016/j.ceb.2015.06.007
23. Jacquemet G, Stubb A, Saup R, Miihkinen M, Kremneva E, Hamidi H et al (2019) Filopodome Mapping Identifies p130Cas as a Mechanosensitive Regulator of Filopodia Stability. Curr Biol 29(202–216):e207. https://doi.org/10.1016/j.cub.2018.11.053
24. Jontes JD, Smith SJ (2000) Filopodia, spines, and the generation of synaptic diversity. Neuron 27:11–14. https://doi.org/10.1016/s0896-6273(00)00003-9
25. Kegel-Gleason KB (2013) Huntingtin interactions with membrane phospholipids: strategic targets for therapeutic intervention? J Huntingtons Dis 2:239–250. https://doi.org/10.3233/JHD-130068
26. Kegel KB, Meloni AR, Yi Y, Kim YJ, Doyle E, Cuiffo BG et al (2002) Huntingtin is present in the nucleus, interacts with the

transcriptional corepressor C-terminal binding protein, and represses transcription. J Biol Chem 277:7466–7476. https://doi.org/10.1074/jbc.M103946200
27. Kegel KB, Sapp E, Alexander J, Valencia A, Reeves P, Li X et al (2009) Polyglutamine expansion in huntingtin alters its interaction with phospholipids. J Neurochem 110:1585–1597. https://doi.org/10.1111/j.1471-4159.2009.06255.x
28. Kegel KB, Sapp E, Yoder J, Cuiffo B, Sobin L, Kim YJ et al (2005) Huntingtin associates with acidic phospholipids at the plasma membrane. J Biol Chem 280:36464–36473. https://doi.org/10.1074/jbc.M503672200
29. Khan RI, Yazawa T, Anisuzzaman AS, Semba S, Ma Y, Uwada J et al (2014) Activation of focal adhesion kinase via M1 muscarinic acetylcholine receptor is required in restitution of intestinal barrier function after epithelial injury. Biochim Biophys Acta 1842:635–645. https://doi.org/10.1016/j.bbadis.2013.12.007
30. Kim D, Jeon J, Cheong E, Kim DJ, Ryu H, Seo H et al (2016) Neuroanatomical visualization of the impaired striatal connectivity in huntington's disease mouse model. Mol Neurobiol 53:2276–2286. https://doi.org/10.1007/s12035-015-9214-2
31. Kuemmerle S, Gutekunst CA, Klein AM, Li XJ, Li SH, Beal MF et al (1999) Huntington aggregates may not predict neuronal death in Huntington's disease. Ann Neurol 46:842–849
32. Kulkarni VA, Firestein BL (2012) The dendritic tree and brain disorders. Mol Cell Neurosci 50:10–20. https://doi.org/10.1016/j.mcn.2012.03.005
33. Kwan W, Trager U, Davalos D, Chou A, Bouchard J, Andre R et al (2012) Mutant huntingtin impairs immune cell migration in Huntington disease. J Clin Invest 122:4737–4747. https://doi.org/10.1172/JCI64484
34. Labbadia J, Morimoto RI (2013) Huntington's disease: underlying molecular mechanisms and emerging concepts. Trends Biochem Sci 38:378–385. https://doi.org/10.1016/j.tibs.2013.05.003
35. Lee J, Hong YK, Jeon GS, Hwang YJ, Kim KY, Seong KH et al (2012) ATRX induction by mutant huntingtin via Cdx2 modulates heterochromatin condensation and pathology in Huntington's disease. Cell Death Differ 19:1109–1116. https://doi.org/10.1038/cdd.2011.196
36. Lee J, Hwang YJ, Kim Y, Lee MY, Hyeon SJ, Lee S et al (2017) Remodeling of heterochromatin structure slows neuropathological progression and prolongs survival in an animal model of Huntington's disease. Acta Neuropathol 134:729–748. https://doi.org/10.1007/s00401-017-1732-8
37. Lee J, Hwang YJ, Shin JY, Lee WC, Wie J, Kim KY et al (2013) Epigenetic regulation of cholinergic receptor M1 (CHRM1) by histone H3K9me3 impairs Ca(2+) signaling in Huntington's disease. Acta Neuropathol 125:727–739. https://doi.org/10.1007/s00401-013-1103-z
38. Li H, Li SH, Johnston H, Shelbourne PF, Li XJ (2000) Amino-terminal fragments of mutant huntingtin show selective accumulation in striatal neurons and synaptic toxicity. Nat Genet 25:385–389. https://doi.org/10.1038/78054
39. Li H, Li SH, Yu ZX, Shelbourne P, Li XJ (2001) Huntingtin aggregate-associated axonal degeneration is an early pathological event in Huntington's disease mice. J Neurosci 21:8473–8481
40. Li JY, Conforti L (2013) Axonopathy in Huntington's disease. Exp Neurol 246:62–71. https://doi.org/10.1016/j.expneurol.2012.08.010
41. Li SH, Li XJ (2004) Huntingtin-protein interactions and the pathogenesis of Huntington's disease. Trends Genet 20:146–154. https://doi.org/10.1016/j.tig.2004.01.008
42. Lietha D, Cai X, Ceccarelli DF, Li Y, Schaller MD, Eck MJ (2007) Structural basis for the autoinhibition of focal adhesion kinase. Cell 129:1177–1187. https://doi.org/10.1016/j.cell.2007.05.041
43. Lin YC, Koleske AJ (2010) Mechanisms of synapse and dendrite maintenance and their disruption in psychiatric and neurodegenerative disorders. Annu Rev Neurosci 33:349–378. https://doi.org/10.1146/annurev-neuro-060909-153204
44. Maat-Schieman ML, Dorsman JC, Smoor MA, Siesling S, Van Duinen SG, Verschuuren JJ et al (1999) Distribution of inclusions in neuronal nuclei and dystrophic neurites in Huntington disease brain. J Neuropathol Exp Neurol 58:129–137. https://doi.org/10.1097/00005072-199902000-00003
45. Mattila PK, Lappalainen P (2008) Filopodia: molecular architecture and cellular functions. Nat Rev Mol Cell Biol 9:446–454. https://doi.org/10.1038/nrm2406
46. Milnerwood AJ, Raymond LA (2010) Early synaptic pathophysiology in neurodegeneration: insights from Huntington's disease. Trends Neurosci 33:513–523. https://doi.org/10.1016/j.tins.2010.08.002
47. Mitra SK, Hanson DA, Schlaepfer DD (2005) Focal adhesion kinase: in command and control of cell motility. Nat Rev Mol Cell Biol 6:56–68. https://doi.org/10.1038/nrm1549
48. Mitra SK, Schlaepfer DD (2006) Integrin-regulated FAK-Src signaling in normal and cancer cells. Curr Opin Cell Biol 18:516–523. https://doi.org/10.1016/j.ceb.2006.08.011
49. Moeller ML, Shi Y, Reichardt LF, Ethell IM (2006) EphB receptors regulate dendritic spine morphogenesis through the recruitment/phosphorylation of focal adhesion kinase and RhoA activation. J Biol Chem 281:1587–1598. https://doi.org/10.1074/jbc.M511756200
50. Murmu RP, Li W, Holtmaat A, Li JY (2013) Dendritic spine instability leads to progressive neocortical spine loss in a mouse model of Huntington's disease. J Neurosci 33:12997–13009. https://doi.org/10.1523/JNEUROSCI.5284-12.2013
51. Murphy KP, Carter RJ, Lione LA, Mangiarini L, Mahal A, Bates GP et al (2000) Abnormal synaptic plasticity and impaired spatial cognition in mice transgenic for exon 1 of the human Huntington's disease mutation. J Neurosci 20:5115–5123
52. Navarro AI, Rico B (2014) Focal adhesion kinase function in neuronal development. Curr Opin Neurobiol 27:89–95. https://doi.org/10.1016/j.conb.2014.03.002
53. Renaudin A, Lehmann M, Girault J, McKerracher L (1999) Organization of point contacts in neuronal growth cones. J Neurosci Res 55:458–471. https://doi.org/10.1002/(SICI)1097-4547(19990215)55:4%3c458::AID-JNR6%3e3.0.CO;2-D
54. Rico B, Beggs HE, Schahin-Reed D, Kimes N, Schmidt A, Reichardt LF (2004) Control of axonal branching and synapse formation by focal adhesion kinase. Nat Neurosci 7:1059–1069. https://doi.org/10.1038/nn1317
55. Ross CA, Tabrizi SJ (2011) Huntington's disease: from molecular pathogenesis to clinical treatment. Lancet Neurol 10:83–98. https://doi.org/10.1016/s1474-4422(10)70245-3
56. Sainath R, Gallo G (2015) Cytoskeletal and signaling mechanisms of neurite formation. Cell Tissue Res 359:267–278. https://doi.org/10.1007/s00441-014-1955-0
57. Saudou F, Finkbeiner S, Devys D, Greenberg ME (1998) Huntingtin acts in the nucleus to induce apoptosis but death does not correlate with the formation of intranuclear inclusions. Cell 95:55–66. https://doi.org/10.1016/s0092-8674(00)81782-1
58. Saudou F, Humbert S (2016) The Biology of Huntingtin. Neuron 89:910–926. https://doi.org/10.1016/j.neuron.2016.02.003
59. Seong J, Ouyang M, Kim T, Sun J, Wen PC, Lu S et al (2011) Detection of focal adhesion kinase activation at membrane microdomains by fluorescence resonance energy transfer. Nat Commun 2:406. https://doi.org/10.1038/ncomms1414
60. Seong J, Tajik A, Sun J, Guan JL, Humphries MJ, Craig SE et al (2013) Distinct biophysical mechanisms of focal adhesion kinase mechanoactivation by different extracellular matrix

proteins. Proc Natl Acad Sci USA 110:19372–19377. https://doi.org/10.1073/pnas.1307405110
61. Shen K, Cowan CW (2010) Guidance molecules in synapse formation and plasticity. Cold Spring Harb Perspect Biol 2:a001842. https://doi.org/10.1101/cshperspect.a001842
62. Shi Y, Pontrello CG, DeFea KA, Reichardt LF, Ethell IM (2009) Focal adhesion kinase acts downstream of EphB receptors to maintain mature dendritic spines by regulating cofilin activity. J Neurosci 29:8129–8142. https://doi.org/10.1523/JNEUROSCI.4681-08.2009
63. Stauffer TP, Ahn S, Meyer T (1998) Receptor-induced transient reduction in plasma membrane PtdIns(4,5)P2 concentration monitored in living cells. Curr Biol 8:343–346. https://doi.org/10.1016/s0960-9822(98)70135-6
64. Szebenyi G, Morfini GA, Babcock A, Gould M, Selkoe K, Stenoien DL et al (2003) Neuropathogenic forms of huntingtin and androgen receptor inhibit fast axonal transport. Neuron 40:41–52. https://doi.org/10.1016/s0896-6273(03)00569-5
65. Tao M, Pandey NK, Barnes R, Han S, Langen R (2019) Structure of Membrane-Bound Huntingtin Exon 1 Reveals Membrane Interaction and Aggregation Mechanisms. Structure 27(1570–1580):e1574. https://doi.org/10.1016/j.str.2019.08.003
66. Tomar A, Schlaepfer DD (2009) Focal adhesion kinase: switching between GAPs and GEFs in the regulation of cell motility. Curr Opin Cell Biol 21:676–683. https://doi.org/10.1016/j.ceb.2009.05.006
67. Tourette C, Li B, Bell R, O'Hare S, Kaltenbach LS, Mooney SD et al (2014) A large scale Huntingtin protein interaction network implicates Rho GTPase signaling pathways in Huntington disease. J Biol Chem 289:6709–6726. https://doi.org/10.1074/jbc.M113.523696
68. Tousley A, Iuliano M, Weisman E, Sapp E, Richardson H, Vodicka P et al (2019) Huntingtin associates with the actin cytoskeleton and alpha-actinin isoforms to influence stimulus dependent morphology changes. PLoS ONE 14:e0212337. https://doi.org/10.1371/journal.pone.0212337
69. Trettel F, Rigamonti D, Hilditch-Maguire P, Wheeler VC, Sharp AH, Persichetti F et al (2000) Dominant phenotypes produced by the HD mutation in STHdh(Q111) striatal cells. Hum Mol Genet 9:2799–2809. https://doi.org/10.1093/hmg/9.19.2799
70. Turner CE (2000) Paxillin and focal adhesion signalling. Nat Cell Biol 2:E231-236. https://doi.org/10.1038/35046659
71. Usdin MT, Shelbourne PF, Myers RM, Madison DV (1999) Impaired synaptic plasticity in mice carrying the Huntington's disease mutation. Hum Mol Genet 8:839–846. https://doi.org/10.1093/hmg/8.5.839
72. Valiente M, Ciceri G, Rico B, Marin O (2011) Focal adhesion kinase modulates radial glia-dependent neuronal migration through connexin-26. J Neurosci 31:11678–11691. https://doi.org/10.1523/JNEUROSCI.2678-11.2011
73. Vonsattel JP, Myers RH, Stevens TJ, Ferrante RJ, Bird ED, Richardson EP Jr (1985) Neuropathological classification of Huntington's disease. J Neuropathol Exp Neurol 44:559–577. https://doi.org/10.1097/00005072-198511000-00003
74. Ziv NE, Garner CC (2004) Cellular and molecular mechanisms of presynaptic assembly. Nat Rev Neurosci 5:385–399. https://doi.org/10.1038/nrn1370